

# Extraction of straight field roads between farmlands based on agricultural vehicle-mounted LiDAR

Lili Yang<sup>1,2</sup>, Yuanyuan Xu<sup>1,2</sup>, Yajie Liang<sup>1,2</sup>, Jia Qin<sup>1,2</sup>, Yuanbo Li<sup>1,2</sup>, Xinxin Wang<sup>1,2</sup>,  
Weixin Zhai<sup>1,2</sup>, Long Wen<sup>1,2</sup>, Zhibo Chen<sup>1,2</sup>, Caicong Wu<sup>1,2\*</sup>

(1. College of Information and Electrical Engineering, China Agricultural University, Beijing 100083, China;

2. Key Laboratory of Agricultural Machinery Monitoring and Big Data Applications, Ministry of Agriculture and Rural Affairs, Beijing 100083, China)

**Abstract:** The application of autonomous agricultural vehicles is gaining popularity as a way to increase production efficiency and lower operational costs. To achieve high performance, perception tasks (such as obstacle detection, road extraction, and drivable area extraction) are of great importance. Compared with structured roads, field roads between farmlands, including unstructured roads and semi-structured roads, are unfavorable for autonomous agricultural vehicle driving due to their bumpiness and unstructured nature. This study proposed an extraction method for the straight field roads between farmlands. The proposed method was based on the point cloud data acquired by LiDAR (Velodyne VLP-16) mounted on a John Deere 1204 6B-1204 tractor. The proposed method has three aspects: Euclidean Clustering-based extraction, boundary-based extraction, and road point cloud curve segment modification. Firstly, Euclidean Clustering with K-Dimensional (KD)-Tree data structure was adopted to extract the road curve segments close to the LiDAR composed of road points. Secondly, the boundary lines constraint was constructed to extract the distant road curve segments. Thirdly, the local distance ratio was used to modify the extracted road curve segments. The average extraction accuracy for both semi-structured and unstructured roads exceeded 98%, and the false positive rate (FPR) was less than 0.5%. These experimental findings demonstrated that the proposed road extraction method was precise and effective. The proposed method of this study can be applied to enhance the perception ability of autonomous agricultural vehicles thereby increasing the efficiency and safety of field road driving.

**Keywords:** road extraction, straight field road, autonomous agricultural vehicle, LiDAR, farmland

**DOI:** 10.25165/j.ijabe.20221505.6933

**Citation:** Yang L L, Xu Y Y, Liang Y J, Qin J, Li Y B, Wang X X, et al. Extraction of straight field roads between farmlands based on agricultural vehicle-mounted LiDAR. *Int J Agric & Biol Eng*, 2022; 15(5): 155–162.

## 1 Introduction

Due to shortage and increasing labor expenses in agricultural operations, research on autonomous control of an agricultural vehicle is extremely important in China<sup>[1]</sup>. Several types of autonomous vehicles are used in agricultural operations. As a result, crop detection and picking<sup>[2,3]</sup>, plant growth monitoring, path

tracking for vehicles in the greenhouse<sup>[4]</sup>, perception for autonomous driving, and obstacle detection<sup>[5]</sup> have been largely studied. As a critical component of a driverless agricultural vehicle, the perception of field roads in real-time via data collected by online sensors using cameras and LiDAR is critical for vehicle localization, path planning, and environmental planning<sup>[6]</sup>.

A LiDAR swipes the environment with high frequency, gathering 3D spatial information and unaffected by the sunlight. This is a sensor with the benefits of high measurement precision, resistance to active interference, and dynamic detection<sup>[7]</sup>. Therefore, it is extensively applied in agricultural scenarios, especially road extraction tasks. LiDAR extracts roads through five major approaches, i.e., image-based method, grid-based method, voxel-based method, point-based method, and curve segment-based method. After the point cloud is projected as images, the road point cloud is extracted using well-developed image processing techniques. However, part of the three-dimensional spatial information disappeared<sup>[8-11]</sup>. The grid-based methods reduce data dimensionality, and the accuracy of the road extraction could reach 95.61% in a city scenario<sup>[12-17]</sup>. Due to the availability of regular data, the voxel-based road extraction methods require few calculations with limited adaptability, while their accuracy could exceed 93%<sup>[18,19]</sup>. The point-based road extraction method obtains favorable features to distinguish road points from non-road points by calculating the distance or height difference from neighboring points, achieving an accuracy of 89.3% on structured road scenarios in the city.

**Received date:** 2021-07-26 **Accepted date:** 2022-06-18

**Biographies:** Lili Yang, PhD, Associate Professor, research interest: big data mining of agricultural machinery, computer vision, virtual plant modeling, intelligent information processing, Email: llyang@cau.edu.cn; Yuanyuan Xu, MS, research interest: perception of autonomous driving, Email: s20203081484@cau.edu.cn; Yajie Liang, PhD, research interest: unmanned agricultural machinery navigation and multimachine cooperative operation, Email: liangyajie@cau.edu.cn; Jia Qin, MS, research interest: perception of autonomous driving, Email: janeqin@cau.edu.cn; Yuanbo Li, MS, research interest: perception of autonomous driving, Email: yeqianchen@cau.edu.cn; Xinxin Wang, MS, research interest: big data mining of agricultural machinery, Email: 939994970@qq.com; Weixin Zhai, PhD, Associate Professor, research interest: big data of spatio temporal, big data mining of agricultural machinery, cartography and geographic information system, and noctilucous remote sensing. Email: zhaiweixin@cau.edu.cn; Long Wen, MS, research interest: control of tractor autonomous driving, Email: wl@cau.edu.cn; Zhibo Chen, PhD, research interest: autonomous driving, Email: chenzb@cau.edu.cn.

\***Corresponding author:** Caicong Wu, PhD, Professor, research interest: unmanned driving and autonomous operation of agricultural machinery, big data mining of agricultural machinery. College of Information and Electrical Engineering, China Agricultural University, Beijing 100083, China. Tel: +86-13810521813, Email: wucc@cau.edu.cn.

Nonetheless, it only considers the local feature of each point<sup>[20]</sup>. In curve segment-based methods, segments comprise the point cloud, and the road curve segments are extracted by analyzing the relationship in space or morphological connection in the curve segments. It had a high degree of flexibility and utilizes the overall differences between the road and the non-road segments; its accuracy can reach 90.94% in unstructured road areas<sup>[21,22]</sup>.

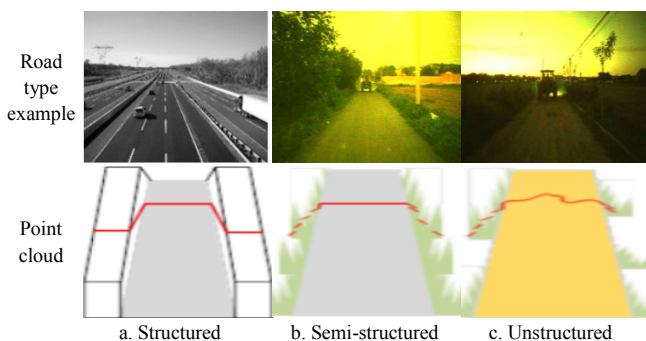
The above approaches have corresponding benefits for road extraction tasks in different scenarios, including structured roads in the city or bumpy roads, but require height differences or regular features at the boundaries. However, they are limited in field road extraction with slight height changes around the road boundary. When extracting roads, it is important to consider details and overall differences between the road and non-road point cloud, and the context of the road points. Yan et al.<sup>[23]</sup> proposed a field road extraction approach based on sharp changes around the boundary. Nevertheless, the method is only applicable to the data gained by LiDAR with four or fewer scan channels and is limited by large road bumps.

The road boundary is blurred and has discontinuous vegetation at various heights and even a bumpy surface. These factors complicate road extraction from field roads. In the structured road scenario, the elevations and angles formed by three adjacent points of the same scan laser are common regular features of boundary points<sup>[24]</sup>. However, they are not suitable for field roads. This work proposed a road extraction method for semi-structured and unstructured field roads in agricultural areas.

## 2 Material and method

### 2.1 Data acquisition

Figure 1 presents three road types and their corresponding point cloud. They include structured road (SR) in Figure 1a, semi-structured road (SSR) in Figure 1b, and unstructured road (UR) in Figure 1c.



Note: The points in red are of the same scan line. The road surface in gray is flat, while yellow is bumpy.

Figure 1 Three types of road and their corresponding point cloud

The roads in the city are SR with continuous and regular road boundaries on flat surface, including curbstones higher than the ground. However, the SSR and the UR lack regularized boundaries of structured roads, but with weeds of different heights along the road. The shape of the road boundary appears irregular. For the UR, the changes in height of the boundary, similar to that of the road surface, make it more complex than SSR. Generally, the latter two cases are common in agricultural scenarios.

The data collection was conducted in Miyun District, Beijing. The types of roads collected included the SSR and the UR. The data were collected by the sensors mounted on the JD1204 tractor (6B-1204, John Deere, USA). The sensors were installed in a favorable mounting position (Figure 2). Considering the stability

and safety of the installation location as well as the vehicle outline, the directional and positioning antennas are mounted on the vehicle roof; GNSS/IMU (CGI-610, CHCNV, China) and camera (BFS-PGE-23S3C-C, FLIR, America) are positioned in front of the top of the vehicle counterweight, and the Velodyne VLP-16 (VLP-16, Velodyne, USA) is mounted in front of the bottom of the counterweight. The calibrations between each pair of sensors are conducted.



Figure 2 Data acquisition equipment

The relationships between the detection area, blind area, and the height of the LiDAR are

$$L = \frac{h}{\tan(\alpha)} \quad (1)$$

where,  $L$  represents the blind coverage area near the ground in front of the LiDAR, 4.48 m;  $h$  represents the vertical height from the optical center of the LiDAR to the ground, 1.24 m. The LiDAR sensor by Velodyne features up to 16 lasers vertically aligned from  $+\alpha$  to  $-\alpha$  ( $\alpha$  is  $15^\circ$ ), and its rotating head delivers a horizontal field of view foreground of  $180^\circ$  in Figure 2, with horizontal resolution at  $\theta_{\text{hor}}$  ( $0.2^\circ$ ). Therefore, half of the scan lasers scan the ground to obtain the furthest detecting distance over 25 m, sufficient for road extraction in agricultural scenarios, where the vehicle's speed is no more than 25 km/h. The other half of the lasers perceive the obstacles or something else over the ground. The positive direction of the  $x$ -axis of the LiDAR is parallel to the vehicle, to the front; the  $y$ -axis is perpendicular horizontally to the  $x$ -axis, to the left; and the  $z$ -axis is vertical to the ground, to the upward.

### 2.2 Road extraction method

The extraction of the field roads is shown in Figure 3. It is a sequential execution.

First, the original point cloud is filtered by the Region of Interest (ROI) and ordered. Afterward, the curve segments comprising the road point cloud near the LiDAR are extracted by Euclidean Clustering. Additional steps are required for distant segments. Then, the road boundary candidate points are extracted and smoothed to obtain the boundary points. Ordinary Least Square (OLS)<sup>[25]</sup> methods are applied to fit the straight lines of the road boundary. Road curve segments farther away from the LiDAR are extracted based on the boundary lines. Moreover, Euclidean Clustering and boundary limitation are accompanied by curve segment modification, yielding a more accurate result.

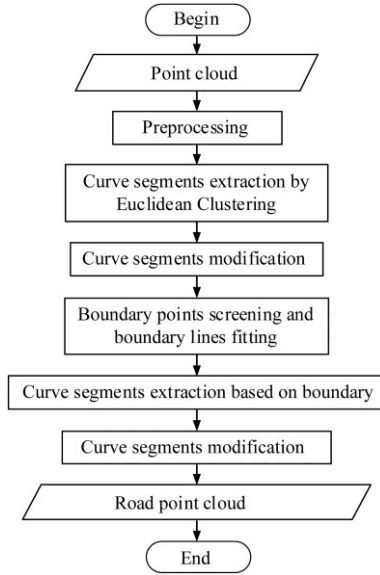


Figure 3 Pipeline of road extraction method of this study

### 2.2.1 Data preprocessing

More attention should be paid to the area covering the road but not the one farther away from the road area. The point cloud in the region of interest (ROI) is defined as,

$PC_{ROI} = \{p | x_p \leq x_{max}, x_p \geq x_{min}, y_p \leq y_{max}, y_p \geq y_{min}, z_p \leq z_{max}, z_p \geq z_{min}\}$  (2) where,  $p$  represents one single point,  $x_{min}$  and  $x_{max}$  limit the scope in the front along the  $x$ -axis (length of the ROI).  $y_{min}$  and  $y_{max}$  limit the scope from the right to left sides along the  $y$ -axis (width of the ROI).  $z_{min}$  and  $z_{max}$  limit the scope from the bottom to the top along the  $z$ -axis (height of the ROI). Then the division of  $PC_{ROI}$  is conducted as,

$$\text{channel}_p = \frac{\left( \arctan \frac{z_p}{\sqrt{x_p^2 + y_p^2}} \right) + \alpha}{2} \quad (3)$$

$$PC_k = \{p | \text{channel}_p = k, p \in PC_{ROI}\} \quad (4)$$

$$PC_{ROI} = \{PC_0, PC_1, PC_2, \dots, PC_{15}\} \quad (5)$$

where,  $\text{channel}_p$  represents the channel of the point  $p$ ;  $PC_k$  represents point cloud where each point's  $\text{channel}_p$  equals  $k$ , whose value range is indicated in Table 1, varying from 0 to 15 according to point's vertical angle (Table 1);  $PC_{ROI}$  are divided into 16 groups of point clouds according to points'  $\text{channel}_p$ . All the points in every division  $PC_k$  are arranged in order by the value of the  $y$ -axis. The points of each division are then distributed from the left to the vehicle's right. This is because an orderly arrangement is critical to the modification part discussed later.

**Table 1 Point's vertical angle and the corresponding  $\text{channel}_p$**

$\text{channel}_p$	Vertical angle of $p/(\circ)$	$\text{channel}_p$	Vertical angle of $p/(\circ)$
0	-15	8	1
1	-13	9	3
2	-11	10	5
3	-9	11	7
4	-7	12	9
5	-5	13	11
6	-3	14	13
7	-1	15	15

### 2.2.2 Extraction by Euclidean Clustering

The distance between points in the curve segments on the road surface differs from the distance between other objects outside the road. As the UR is more complex than the SSR mentioned before,

take the UR as the example indicated in Figure 4.

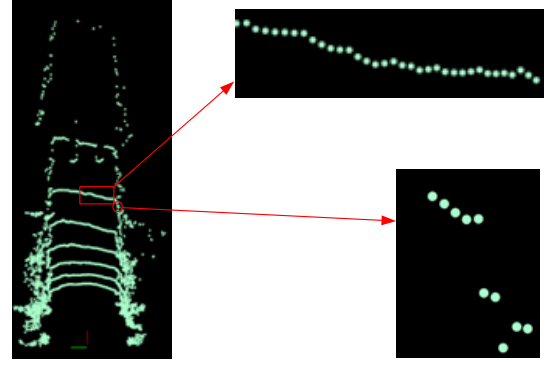


Figure 4 Illustration of the distribution of point clouds on the road and road boundary

The curve segments of the field road are not as smooth as the curve segments on the frictionless surface but more regularized and denser than that of the non-road outside the boundary. Therefore, part of the curve segments connected by the road points can be extracted based on the spatial distance between points. Unlike the road extraction method based on the angle between three adjacent points<sup>[26]</sup>, the clustering-based method considers the continuity and bumpiness of the road surface by the proper distance threshold  $d_{thre}$  calculated by Equation (6).

$$d_{thre} = \frac{h}{\sin \alpha} \times \frac{\theta_{hor}}{180} \times \pi + \delta \quad (6)$$

where,  $\theta_{hor}$ ,  $h$ , and  $\delta$  determine the distance threshold used in the clustering;  $\delta$  is set as the redundancy, which accounts for the bumpiness of the road surface. The commonly employed cluster methods include Euclidean Clustering and Density-Based Spatial Clustering of Applications with Noise (DBSCAN) Clustering. In contrast with DBSCAN Clustering with iterations and the initial seed point<sup>[27]</sup>, only the distance threshold is necessary for Euclidean Clustering, with stronger adaptability<sup>[28]</sup>. Euclidean Clustering is utilized to obtain the curve segments, and the K-Dimensional (KD)-Tree algorithm is employed to speed up the search of neighborhood points.

Nevertheless, the fixed threshold may result in the missing extraction of the distant road curve segments. So to obtain the whole information on the field road, the missed distant road curve segments should be extracted by the following step.

### 2.2.3 Boundary points screening and boundary lines fitting

The missed farther segments will be obtained by the boundary line restriction. The left and right endpoints of the extracted curve segments in Section 2.2.2 are considered candidate boundary points for the two sides of the road. To ensure the fitting of the boundary line is away from the impact of the outlier, the candidate boundary points are screened before fitting boundary lines. Unlike the methods based on searching-based<sup>[29]</sup> and road width-based boundary point generation<sup>[30]</sup>, this study generated boundary points from segments in a simpler and more flexible way.

The left and right boundary candidate points of the road are traversed, respectively, and the sum of the distance parallel to the  $y$ -axis of each point is calculated such that

$$f_i = \sum_{j=1}^m |y_{p_i} - y_{p_j}|, (i \neq j, i \in [1, m], j \in [1, m]) \quad (7)$$

$$f_{thre} = \frac{(\sum_{i=1}^m f_i - f_{max} - f_{min})}{m - 2} \quad (8)$$

where,  $f_i$  represents the sum of distance in the  $y$ -axis direction of point  $p_i$  with all other candidate points;  $m$  represents the number of endpoints on the same side of extracted segments from the Euclidean Clustering, varying with the results of Euclidean Clustering;  $y_{p_i}$  and  $y_{p_j}$  are the  $y$ -axes coordinate values referring to two different candidate points  $p_i$  and  $p_j$  out of  $m$  points, on the same side of the boundary, arbitrarily. The max and the min in the set are excluded, and the threshold  $f_{thre}$  is set to the average of the remained ones, making sure of two points at least on each side. When  $f_i$  exceeds the threshold  $f_{thre}$ , point  $p_i$  is considered the outlier and deleted. This is because the distance difference along the  $y$ -axis between three boundary points on the same side should be small in the road of low curvature. The final road boundary points are obtained after that the distance ratio between every three boundary candidate points satisfies the threshold  $f_{thre}$ . Then the boundary lines are fitted by OLS, and the remained road curve segments comprising road points between both boundaries can be extracted.

#### 2.2.4 Curve segments modification

The points of the grass along the boundary would likely be mistakenly clustered into the road curve segments, which are extracted following the preceding procedures.

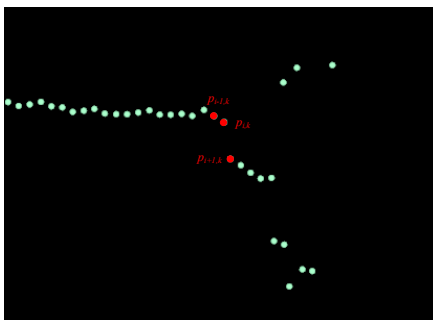
In Figure 5,  $p_{i-1,k}$ ,  $p_{i,k}$ ,  $p_{i+1,k}$  are three points from the same laser channel  $k$  in adjacency; the first two belong to the road, while the last belongs to the grass outside the road. Due to the irregularity of the boundary points in the SSR and UR, the distance between  $p_{i-1,k}$  and  $p_{i,k}$  and that of  $p_{i+1,k}$  and  $p_{i,k}$  were significantly different. Therefore, the modification was adopted to correct the curve segments of the road. The local feature of the detail is calculated as follows:

$$d_L = \sqrt{(x_{p_{i,k}} - x_{p_{i-1,k}})^2 + (y_{p_{i,k}} - y_{p_{i-1,k}})^2 + (z_{p_{i,k}} - z_{p_{i-1,k}})^2} \quad (9)$$

$$d_R = \sqrt{(x_{p_{i,k}} - x_{p_{i+1,k}})^2 + (y_{p_{i,k}} - y_{p_{i+1,k}})^2 + (z_{p_{i,k}} - z_{p_{i+1,k}})^2} \quad (10)$$

$$d_{ratio} = \frac{d_L}{d_R} \quad (11)$$

where,  $d_{ratio}$  of a point represents the distance ratio;  $d_L$  represents the Euclidean distance between the point and its left adjacent point, and  $d_R$  represents the distance between the point and its right adjacent point. As illustrated in Figure 5, the distances between the three points vary significantly. Thus, abrupt changes in  $d_{ratio}$  occur around the road boundary. As a result, endpoints of curve segments of the road around the boundary could be modified when the  $d_{ratio}$  exceeds  $d_{ratio\_thre}$ . Therefore, the grass points mistakenly extracted as part of curve segments can be corrected.



Note: UR: Unstructured road, the same as below.

Figure 5 Points around the boundary in UR

#### 2.2.5 Parameter settings

In Table 2, there is a significant change of adjacent points of more than 0.03 m, from  $PC_5$  to  $PC_6$ . Furthermore,  $\delta$  can be set according to changes in the distance between points due to the

bumpiness.  $d_{thre}$  is set based on the above analysis. Because the distance between boundary points along the  $y$ -axis is not large,  $f_{thre}$  is set to allow the tune change between candidate boundary points;  $d_{ratio}$  is calculated by the feature of the boundary points in Figure 5.

Table 3 lists the parameters introduced in the method and their types and values.  $x_{max}$  and  $x_{min}$  were set to 25 m and 0, respectively. Since the braking distance of the vehicle at the maximum speed of 25 km/h is less than 8 m.  $y_{max}$  and  $y_{min}$  were set to 5 m and  $-5$  m, respectively, because the typical road width is 3-5 m;  $z_{max}$  and  $z_{min}$  are determined by the height of the LiDAR and the height difference of the road surface, no more than 1 m.  $d_{thre}$  can be set based on multiple parameters. Assuming that the LiDAR is placed on the horizontal plane at the vertical height  $h$ , the distance between two adjacent points from the same laser channel varies due to the vertical angle of the channel (Table 1), varying from 0.016 m to 0.248 m (Table 2).

**Table 2 Distance between adjacent points from the same laser swiping the ground**

channel <sub>p</sub>	Vertical angle/(°)	Distance between points/m
0	-15	0.016
1	-13	0.018
2	-11	0.022
3	-9	0.027
4	-7	0.035
5	-5	0.050
6	-3	0.083
7	-1	0.248

**Table 3 Parameter list of the straight field road extraction**

Parameter name	Function	Data type	Value
$x_{max}, x_{min}, y_{max}, y_{min}, z_{max}, z_{min}$	Coverage of the ROI (m).	Double	25, 0, 5, -5, 1, -1
$\delta$	The redundancy of the threshold of Euclidean Clustering (m).	Double	0.03-0.05
$d_{thre}$	The threshold of Euclidean Clustering (m).	Double	0.08-0.1
$f_{thre}$	The threshold of the Boundary screening (m).	Double	Adaptive threshold.
$d_{ratio\_thre}$	The threshold of the local distance ratio of the boundary points in the modification part.	Double	2.0-3.0

## 3 Results and discussion

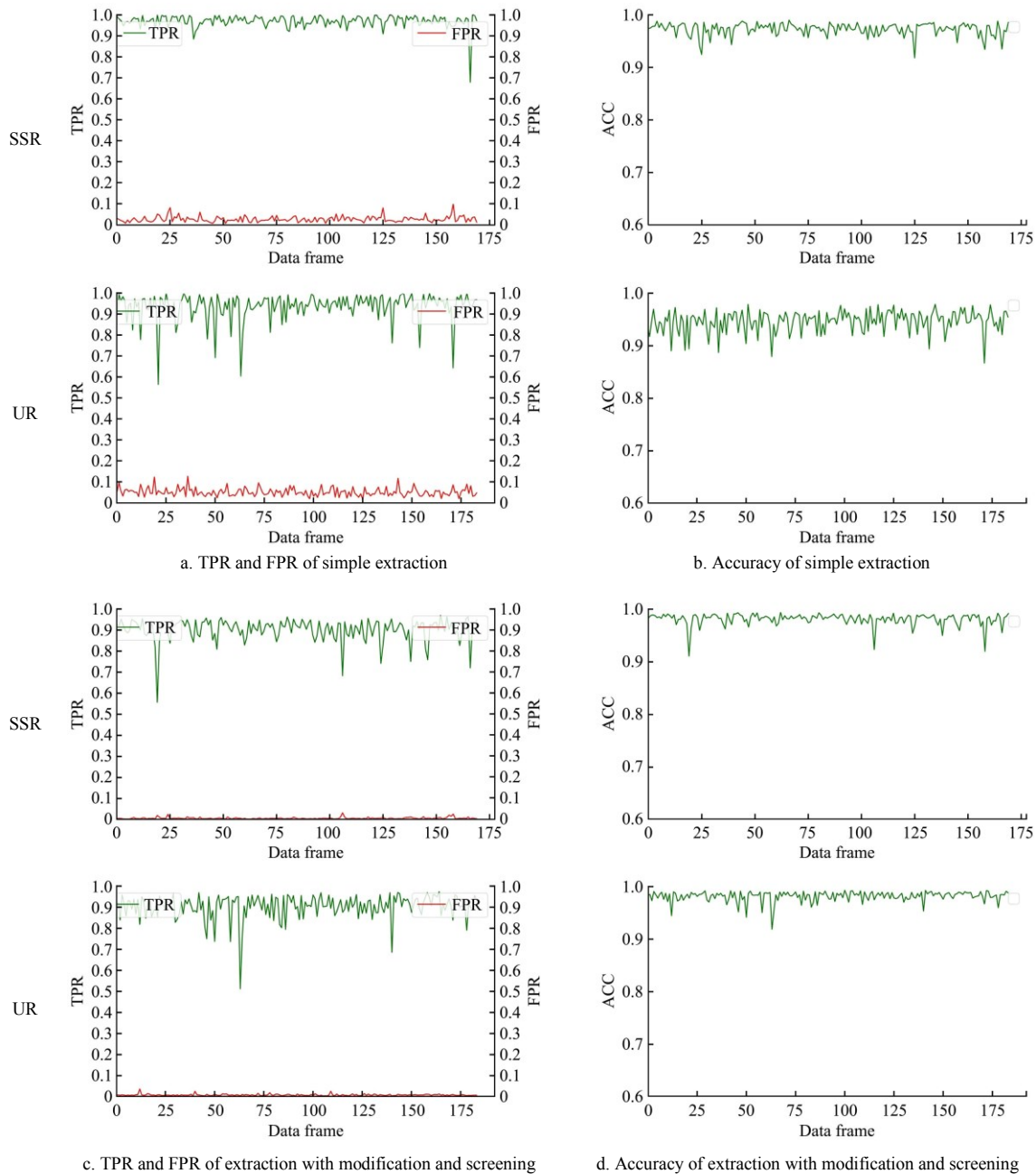
### 3.1 Performance evaluation

Extracting field roads between farmlands is considered a binary classification task of points into the road and the non-road. Similar to their application in the SR extraction tasks, the quantitative evaluations are used by true positive rate (TPR), false positive rate (FPR), accuracy (ACC)<sup>[31,32]</sup>, and Run time (RT). Points belonging to the road are considered positive, while points not belonging to the road are considered negative. Subsequently, each data frame of the point cloud and the averages of the evaluation indices were evaluated.

### 3.2 Results

The experiment was run on a laptop with an i7-9750H 2.60GHz CPU and 16 GB of RAM under the Robot Operation System in Ubuntu 18.04.

All frames of the point cloud for the experiment were annotated by the tools on the platform BasicFinder<sup>[33]</sup>, at point-wise annotation. Each frame was processed, and the results are compared with those of annotated labels. The evaluations are shown in Figure 6.



Note: SSR: Semi-structured road; UR: Unstructured road; TPR: True positive rate; FPR: False positive rate; ACC: Accuracy. The same as below.

Figure 6 Experiment results (TPR, FPR, and ACC) on all frames of simple extraction and extraction with modification and screening

As illustrated in Figure 6, the fluctuations of the evaluation indicator of the road extraction after the modification part and candidate points screening (abbreviated to Extraction with modification and screening) are smaller and smoother. Figures 6a and 6c show that the modification may cause a certain amount of road points to be mistakenly rejected, decreasing the TPR of Extraction with modification and screening in SSR conditions. On the other hand, the FPR of the Extraction with modification and screening remained in a lower state under the SSR and the UR conditions. By comparing the same evaluation indicator in two scenarios, the method performed more stability in the SSR than UR. This is because the road surface was much bumpier in the UR than in SSR, and the technique might be better under the SSR. In both scenarios, the robustness and the stability of the Extraction with modification and screening improved. The average level of the method was determined after evaluating each frame.

In Table 4, a small amount of the experimental data was taken

from a curved road with low curvature, and the majority of data was taken from a straight road. The TPR in the extraction with modification and screening condition decreased by 3.28% and 6.77%. This is because the obstacle inside the road affects the processing of the modification part, resulting in false screening of the road points. Although the TPR decreased, there was a drastic improvement in FPR with Extraction with modification and screening method, dropping from 5.18% to 0.45%. Accuracy in SSR and UR were both more than 98%, while FPR were both less than 0.5%. Therefore, there was a remarkable improvement in the modification part correcting the wrong extraction of the non-road points and the boundary point screening. Compared with the Simple extraction, the added modification and screening part only increased slight time cost.

The overall accuracy of extraction with modification and screening method was higher than that of the Simple extraction method. The extraction accuracy of the Simple extraction was higher in SSR than in UR due to the higher complexity in UR.

However, the average evaluation indicator of the Extraction with modification and screening in both scenarios was similar because the modification part was designed specifically for the common

feature of the boundary in field roads between farmlands. In Figures 7c-7e, the green points represent points of the road, whereas the red points represent the non-road points.

**Table 4 Evaluation indicators of experimental results**

Type	Number of frames	Simple extraction				Extraction with modification and screening			
		TPR <sub>avg</sub> /%	FPR <sub>avg</sub> /%	ACC <sub>avg</sub> /%	RT <sub>avg</sub> /ms	TPR <sub>avg</sub> /%	FPR <sub>avg</sub> /%	ACC <sub>avg</sub> /%	RT <sub>avg</sub> /ms
SSR	170	96.97	2.76	97.21	19	90.20	0.41	98.07	23
UR	184	93.52	5.18	94.62	20	90.24	0.45	98.09	25

Note: SSR: Semi-structured road; UR: Unstructured road; TPR<sub>avg</sub> is the average value of true positive rate (TPR); FPR<sub>avg</sub> is the average value of false positive rate (FPR); ACC<sub>avg</sub> is the average value of accuracy; RT<sub>avg</sub> is the average value of run time (RT).

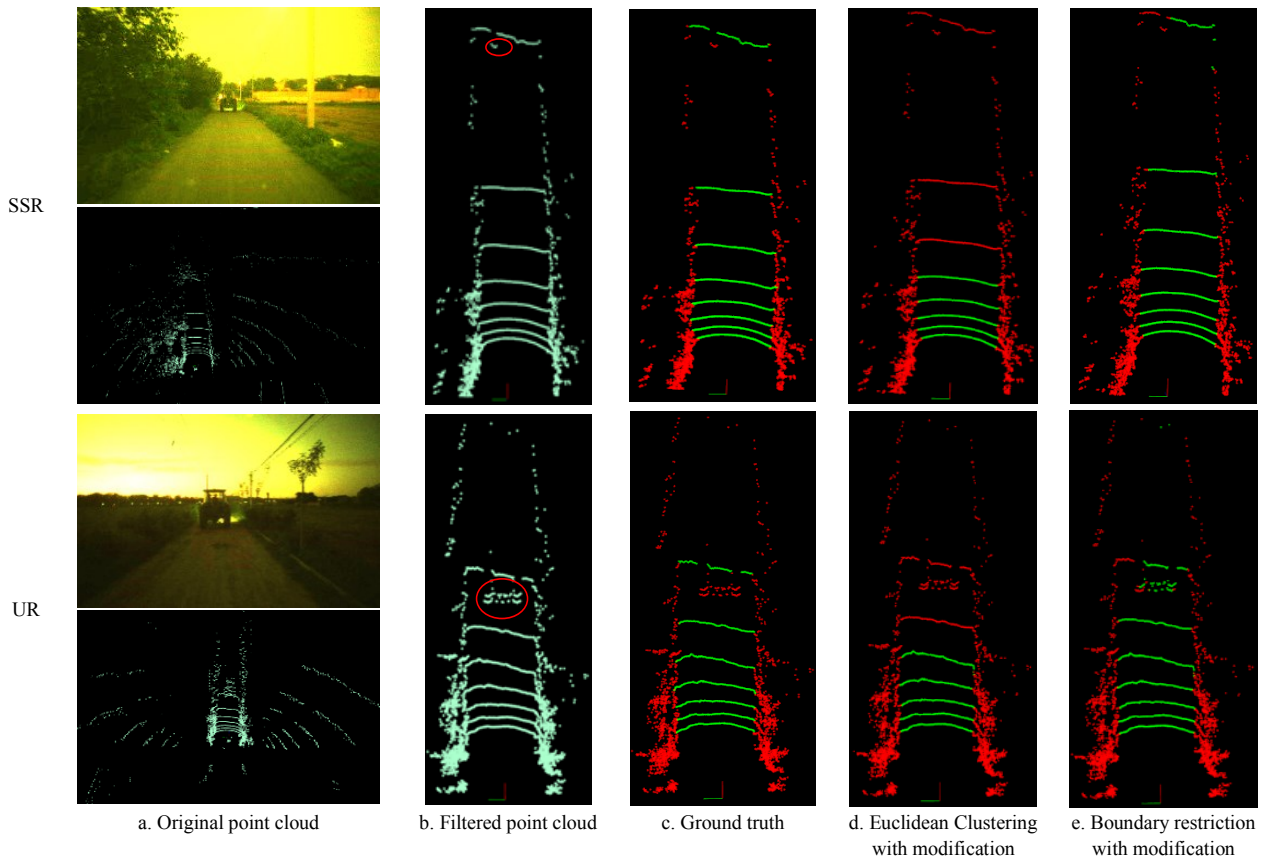


Figure 7 Results of the road extraction in two scenarios

### 3.2.1 Data preprocessing

Figure 7a shows that the points are distributed with coverage of more than one hundred meters long with all the laser scans. After preprocessing, the points decreased by 60%-66%, eliminating numerous noise points and significantly reducing the time consumption of subsequent processing. At the same time, ROI filtering reduces the disturbance from the points unrelated to the road surface and retains the key features of the road surface and boundaries. Although a few obstacles inside the road still exist, as shown by the red circle in Figure 7b, most were eliminated after z-axis filtering. Afterward, all the points from the same laser channel were in order, facilitating the calculation of the  $d_{ratio}$ .

### 3.2.2 Extraction by Euclidean Clustering

As shown in Figure 7c, the road points from the same scan line were more continuous compared with the scattered grass points. By comparing the ground truth. Figure 7d, the Euclidean Clustering was efficiently performed in extracting the road curve segments with a proper threshold of distance for clustering (Equation (6)). The curve segments belonging to the road surface near the LiDAR were extracted. A few points of grass were extracted as a part of the road segments due to a slight difference in

the distance between the non-road points and road boundary points. Therefore, it was difficult to distinguish the non-road points. This problem was solved in the modification part.

Meanwhile, the difference in the distribution of road points in the two scenarios greatly impacted the clustering,  $d_{thre}$  at 0.085 m under the SSR scenario while  $d_{thre}$  at 0.1 m under the UR scenario. With the bumpiness changes in road surface in the UR while driving, the extracted segments after this part varied. It means the farther the point cloud from the LiDAR, the greater the distance between the adjacent points in the curve segment, and the distance between points increases non-linearly. Consequently, Euclidean Clustering with the fixed threshold did not work on the road segments away from the LiDAR, suggesting that relying solely on the clustering method is insufficient and that another process is necessary to solve the problem.

### 3.2.2 Boundary points screening and boundary lines fitting

As shown in Figure 7e, outliers were eliminated after screening. This contributed to the field of boundary line fitting. The fitting lines neatly conformed to the road shape (Figure 8) (the same frame in Figure 7).

In Figure 8, the lines in red represent the result of the

Extraction with modification and screening method, and the lines in green represent the result of the Simple extraction. The space limitations between the two boundary lines varied depending on whether there were points screening and modification parts. After modifying the segments and screening the points, the boundary lines restrained more points inside the road in both scenarios. Although more grass points were extracted, the modification part helped address that.

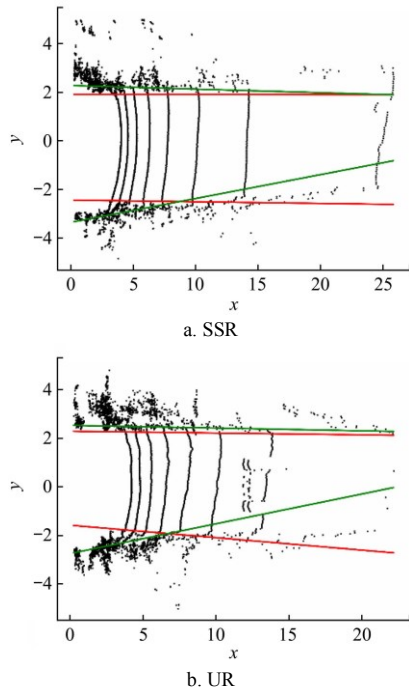


Figure 8 Boundary lines fitting of the extraction with modification and screening and the simple extraction in two scenarios

### 3.2.3 Extraction of curve segments based on boundaries

As illustrated in Figure 7d, curve segments of the road farther away from LiDAR were missing, and the number of missed segments was different in SSR and UR. After extraction restricted by boundary, the segments from the LiDAR in the ROI were contained within. As illustrated in Table 4, in the SSR and the UR scenarios, the road extraction accuracy performed well, and both were above 98% with good results.

### 3.2.4 Modification of curve segments

The results for both scenarios are shown in Figure 7. There are nearly no grass points in the road segments green around the boundaries. Nevertheless, when it met obstacle points inside the road curve segments, the modification part wrongly culled part of the road points near that, as demonstrated by the reduction of the TPR comparing the Simple extraction with the Extraction with modification and screening in Table 4. Moreover, the following are the characteristics of the points in the two scenarios.

In Figure 9, the green points represent  $d_{ratio}$  of the road points, and the red points represent that of the non-road ones. The distance between neighboring points differed despite the points coming from a similar laser channel. However,  $d_{ratio}$  of points was stable inside the road, and the local feature of the point around the road boundary had sharp changes. As shown in Figure 7, only a few grass points outside the road were extracted as the road points. Comparison experiments were performed to demonstrate the performance of the modification part.

By comparing the results in Figure 10a and 10b, most parts of the non-road point cloud mistakenly extracted as the road points (in green), and circled in yellow, were modified into the red correctly.

A few non-road points around the two sides of the boundaries were wrongly extracted; however, with modification, they were filtered. Modification effectively worked on reducing the wrong extraction of the non-road points. As a result, the false extraction of non-road points of the frame was reduced, slightly affecting the fitting of boundary lines. At the same time, this caused the removal of road points close to the road boundary when modifying the endpoints of several road curve segments.

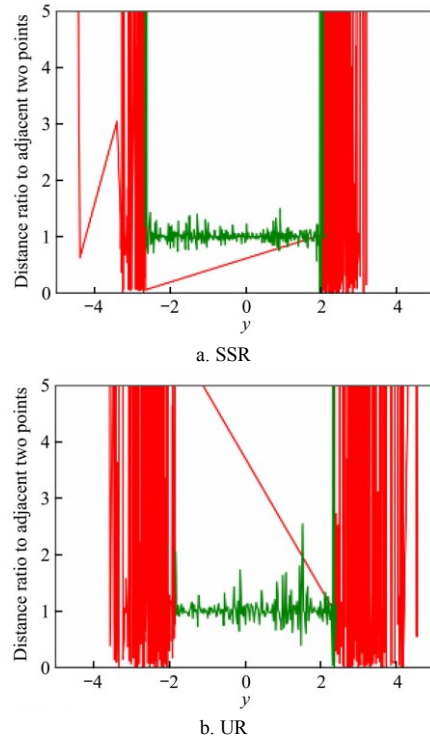


Figure 9  $d_{ratio}$  of each point in two scenarios

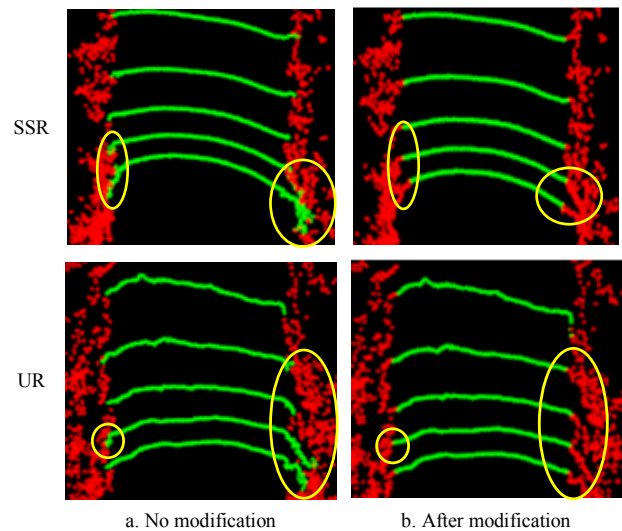


Figure 10 Experiments of the modification in two scenarios

Extraction with modification and screening had a better effect on reducing the false extraction rate of non-road points for field road extraction. In the entire modification, calculating the  $d_{ratio}$  of the points in a small coverage was sufficient, with low time-consuming but high performance. The modification part improved the road extraction by combining the overall difference processing the road curve segments, including Euclidean Clustering and boundary restriction. The proposed method satisfies the real-time requirements and provides accurate road extraction for autonomous agricultural vehicle driving.

## 4 Conclusions

In this study, the proposed extraction method for field roads consists of three stages, including 1) Euclidean Clustering based on the local distance of the road points; 2) modification applying the ratios of the adjacent distance of the road boundary points; 3) boundary lines limitation considering the context of the curve segments comprising the road points. The experimental results show that an average accuracy of over 98% is obtained in the SSR and UR, the average FPR is less than 0.5%, and also achieved high real-time performance of less than 30 ms; this confirms the robustness of the method.

Even if the road had a low curvature, the relationship between the road curve segments within the space appears to be linear; therefore, it was comparable to all segments being determined when the closest segments were determined. The TPR dropped to 90% of the Extraction with modification and screening from 96% of the Simple extraction as the obstacle points inside the road affected the modification part. In addition, the visualization results of the method experimented on curved roads of high curvature conflicted with that on most parts of the experimental data, which was the road of low curvature. This was possible because the line fitting was unsuitable for the curved roads of high curvature. Above all, this study performed well on the extraction of field roads of low curvature and real-time. Since this study considered the obstacles in the setup of the LiDAR, future work should extend to curved road extraction and explore the drivable area of the field roads in agricultural scenarios.

## Acknowledgments

The authors acknowledge that this work was financially supported by the National Key Research & Development Project (Grant No. 2021YFB3901302) and the Beijing Municipal Science and Technology Project (Grant No. Z201100008020008).

## [References]

- [1] Liu X T, Li X L, Xu L J, Chen H, Zhang C S, Sun M Y, et al. Current status and development prospects of agricultural vehicle autonomous driving technology. *Agricultural Vehicle Technology Extension*, 2020; 12: 22–24. (in Chinese)
- [2] Feng X B, He P J, Zhang H X, Yin W Q, Qian Y, Cao P, et al. Rice seeds identification based on back propagation neural network model. *Int J Agric & Biol Eng*, 2019; 12(6): 122–128.
- [3] Zhao X K, Li H, Zhu Q B, Huang M, Guo Y, Qin J W. Automatic sweet pepper detection based on point cloud images using subtractive clustering. *Int J Agric & Biol Eng*, 2020; 13(3): 154–160.
- [4] Wang G J, Wu J, He R, Yang S. A point cloud-based robust road curb detection and tracking method. *IEEE Access*, 2019; 7: 24611–24625.
- [5] Ji C Y, Shen Z Y, Gu B X, Tian G Z, Zhang J. Obstacle detection based on point clouds in application of agricultural navigation. *Transactions of the CSAE*, 2015, 31(7): 173–179.
- [6] Yao L J, Hu D, Zhao C, Yang Z D, Zhang Z. Wireless positioning and path tracking for a mobile platform in greenhouse. *Int J Agric & Biol Eng*, 2021; 14(1): 216–223.
- [7] He Y, Jiang H, Fang H, Wang Y, Liu Y F. Research progress of intelligent obstacle detection methods of vehicles and their application on agriculture. *Transactions of the CSAE*, 2018, 34(9): 21–32.
- [8] Lyu Y C, Bai L, Huang X M. Real-time road segmentation using LiDAR data processing on an FPGA. In: 2018 IEEE International Symposium on Circuits and Systems (ISCAS), Florence: IEEE, 2018; pp.1–5. doi: 10.1109/ISCAS.2018.8351244.
- [9] Paigwar A, Erkent Ö, González D S, Laugier C. GndNet: Fast ground plane estimation and point cloud segmentation for autonomous vehicles. In: 2020 IROS 2020 IEEE/RSJ International Conference on Intelligent Robots and Systems (IROS), 2020; pp.2150–2156. doi: 10.1109/IROS45743.2020.9340979.
- [10] Gao B, Xu A R, Pan Y C, Zhao X J, Yao W, Zhao H J. Off-road drivable area extraction using 3D LiDAR data. 2019 IEEE Intelligent Vehicles Symposium (IV), 2019; pp.1505–1511. doi: 10.1109/IVS.2019.8814143.
- [11] Caltagirone L, Scheidegger S, Svensson L, Wahde M. Fast LiDAR-based road detection using fully convolutional neural networks. 2017 IEEE Intelligent Vehicles Symposium (IV), 2017; pp.1019–1024. doi: 10.1109/IVS.2017.7995848.
- [12] Wang J, Kong B, Wang C, Yang J. An approach of real-time road boundary detection based on HDL-64E lidar. *Journal of Hefei University of Technology (Natural Science)*, 2018, 41(8): 1029–1034. (in Chinese)
- [13] Lu X W. Real-time detection and tracking of mine road boundary lines. Master dissertation. Beijing: University of Chinese Academy of Sciences (School of Artificial Intelligence), 2020; 66p. (in Chinese)
- [14] Tang J L, Lu X W, Ai Y F, Tian B, Chen L. Road detection for autonomous truck in mine environment. In: 2019 IEEE Intelligent Transportation Systems Conference (ITSC), 2019; pp.839–845. doi: 10.1109/ITSC.2019.8917022.
- [15] Lu X W, Ai Y F, Tian B. Real-time mine road boundary detection and tracking for autonomous truck. *Sensors*, 2020; 20(4): 1121. doi: 10.3390/s20041121.
- [16] Chen J H. A study of methods for road extraction from airborne LiDAR data. *Engineering of Surveying and Mapping*, 2020; 29(3): 51–55.
- [17] Byun J, Na K, Seo B, Roh M. Drivable road detection with 3D point cloud based on the MRF for intelligent vehicle. *Field and Service Robotics, Springer Tracts in Advanced Robotics*, 2015; pp.49–60.
- [18] Reina G, Milella A, Rouveure R, Nielsen M, Worst R, Blas M R. Ambient awareness for agricultural robotic vehicles. *Biosystems Engineering*, 2016; 146: 114–132.
- [19] Goga S, Nedevschi S. An approach for segmenting 3D LIDAR data using multi-volume grid structures. In: 2017 IEEE International Conference on Intelligent Computer Communication and Processing (ICCP), 2017; pp.309–315. doi: 10.1109/ICCP.2017.8117022.
- [20] Zhang Y H, Wang J, Wang X N, Dolan J M. Road-segmentation-based curb detection method for self-driving via a 3D-LiDAR sensor. *IEEE Transactions on Intelligent Transportation Systems*, 2018; 19(12): 3981–3991.
- [21] Zhu Z, Liu J L. Graph-based ground segmentation of 3D LIDAR in rough area. In: 2014 IEEE International Conference on Technologies for Practical Robot Applications (TePRA), 2014; pp.1–5. doi: 10.1109/TePRA.2014.6869157.
- [22] Cheng Z Y, Ren G Q, Zhang Y. Ground segmentation from 3D point cloud using features of scanning line segments. *Opto-Electronic Engineering*, 2019; 46(7): 180268. doi: 10.12086/OEE.2019.180268.
- [23] Yan M, Cai Y F, Chen M. A new accessible area detection algorithm in unstructured environment. *Computer & Digital Engineering*, 2019; 47(7): 1652–1661.
- [24] Horváth E, Pozna C, Unger M. Real-time LiDAR-based urban road and sidewalk detection for autonomous vehicles. *Sensors*, 2022; 22(1): 194. doi: 10.3390/s22010194.
- [25] Ordinary Least Square. Available: <https://deeptai.org/machine-learning-glossary-and-terms/ordinary-least-squares>. Accessed on [2021-07-01].
- [26] Fu L M. Drivable area extraction from multiple aliened frames of point cloud. Master dissertation. Wuhan: Wuhan University, 2017; 67p. (in Chinese)
- [27] Zhang C Y, Chen Z H, Han L. Obstacle detection of Lidar based on Improved DBSCAN algorithm. *Laser & Optoelectronics Progress*, 2021; 58(24): 2428005. doi: 10.3788/LOP202158.2428005.
- [28] Chen X Y, Yang Y, Xiang Y F. Measurement of point cloud data segmentation based on Euclidean clustering algorithm. *Bulletin of Surveying and Mapping*, 2017; 11: 27–31, 36. (in Chinese)
- [29] Zhu X K, Gao M J, Li S N. A real-time road boundary detection algorithm based on driverless cars. *Journal of Beijing Union University (Natural Sciences)*, 2015; 29(4): 1–7.
- [30] Li G J, Bao H, Xu C. Real-time road edge extraction algorithm based on 3D-Lidar. *Computer Science*, 2018; 45(9): 294–298. (in Chinese)
- [31] Hao X S. The 3D model simplification technology in virtual reality. Master dissertation. Xi'an: Xidian University, 2007; 53p. (in Chinese)
- [32] Bellone M, Reina G, Caltagirone L, Wahde M. Learning traversability from point clouds in challenging scenarios. *IEEE Transactions on Intelligent Transportation Systems*, 2018; 19(1): 296–305.
- [33] BasicFinder. Available: <https://saas.passport.beisai.com>. Accessed on [2021-07-01].